

Thermal Image and Phase Transitions of Charged AdS Black Holes using Shadow Analysis

A. Belhaj^{1*}, L. Chakhchi^{1†}, H. El Moumni^{2‡}, J. Khalloufi^{3§}, K. Masmarr^{4¶},^{||}

¹ ESMAR, Physics Department, Faculty of Science, Mohammed V University in Rabat, Morocco.

² EPTHE, Physics Department, Faculty of Science, Ibn Zohr University, Agadir, Morocco.

³ LPHEA, FS, Cadi Ayyad University, Marrakech, Morocco.

⁴ Laboratory of High Energy Physics and Condensed Matter Hassan II University
Faculty of Science Ain Chock, Casablanca, Morocco.

September 9, 2020

Abstract

We investigate the relations between the black hole shadow and charged AdS black hole critical behavior in the extended phase space. Using the thermo-shadow formalism built in [1], we reveal that the shadow radius can be considered as an efficient tool to study thermodynamical black hole systems. Based on such arguments, we build a thermal profile by varying the RN-AdS black hole temperature on the shadow silhouette. Among others, the Van der Waals-like phase transition takes place. This could open a new window on the thermal picture of black holes and the corresponding thermodynamics from the observational point of view.

Contents

1	Introduction	2
2	Shadows and thermodynamics of black holes	3
3	Phase transition of charged AdS black hole using shadow formalism	5
4	Thermal profile on the shadow silhouette of RN-AdS black hole	9
5	Conclusion	12

*belhadjadil@fsr.ac.ma

†chakhchi.07@gmail.com

‡hasan.elmoumni@edu.uca.ma (Corresponding author)

§jamalkhalloufi@gmail.com

¶karima.masmarr@edu.uca.ac.ma

|| Authors in alphabetical order, they contributed equally to this work.

1 Introduction

The Event Horizon Telescope (EHT) image has been considered as a relevant achievement of the Einstein theory of gravitation [2–4]. The black hole image, in the center of M87* galaxy, provides huge and immense supports to its existence in the cosmos parallelly with gravitational wave detections by LIGO and Virgo [5]. It has opened a new window to understand the elements of the gravitation theory and brought primordial information concerning jets and matter dynamics around such compact objects. Precisely, the shadow of a black hole can be interpreted as an abundant source of data describing the black hole hairs including the mass, the charge, and the rotation physical parameters. This can be exploited to unveil physical constraints on the gravitational theories [6–8]. More precisely, the black hole shadow corresponds to the gravitational lensing of light around massive objects. Interposing the black hole between an observer and certain sources, it has been observed that not all emitted lights can come to the observer after communication with the strong gravitational field of the black hole. In this way, certain photons collapse into the black hole generating the so called shadow. Many investigations have been elaborated including the seminal works [9, 10] dealing with the shadow of a Schwarzschild black hole and extensions to rotating cases [9–16]. In particular, this direction has been extensively investigated using different ways and methods [17–42].

Recently, it has been remarked that the study of thermodynamic proprieties of black holes, in AdS spacetime, has received remarkable interests [43–60]. Interpreting the cosmological constant in such a space as the pressure of the general thermodynamic system $P = -\frac{\Lambda}{8\pi} = \frac{3\pi}{8\ell^2}$, many interesting results have been obtained for various black hole solutions. Concretely, it has been found a nice interplay between the black hole state parameter and the Van der Waal’s state equation generating a critical phenomenon in AdS spacetime backgrounds.

More recently, such issues have been linked to shadow formalism. In particular, it has been established a direct bridge between the black hole thermodynamical systems and the shadow black holes [1].

The aim of this work is to contribute to these activities by investigating the thermal profile of AdS black hole shadows. Precisely, we study the correlation between the black hole shadows and RN- AdS black hole critical behaviors in the extended phase space. Based on the associated developed analysis, we show that the shadow radius can be considered as an efficient tool to study thermodynamical black hole systems. In particular, we construct a thermal profile by varying the RN-AdS black hole temperature on the shadow silhouette, where the Van der Waals-like phase transition takes place. We expect that this could open a new gate for unveiling the thermal picture of black holes and the corresponding thermodynamics from the observational point of view.

The paper is structured as follows. In section.2, we give a concise review on shadow formalism applied to AdS black holes. In section.3, we show that the Van der Waals-like phase transition in $T - r_h$ persists in $T - r_s$ plane. In section.4, we present a thermal profile of the shadow associated with the RN-AdS black hole. In particular, we show that the oscillation behavior of the temperature characterizing the Van der Waals-like transition can be directly observed in such a thermal picture. The last section is reserved to conclusions and certain open questions.

2 Shadows and thermodynamics of black holes

In this section, we give a concise review on the known results on the black hole shadow and the corresponding thermodynamics being firstly developed in [1]. For more details, we refer to such a work. Indeed, we consider a static spherically symmetric space-time background which can be described by the following line element expression

$$ds^2 = -f(r)dt^2 + \frac{dr^2}{g(r)} + r^2 d\theta^2 + r^2 \sin^2 \theta d\phi^2. \quad (1)$$

$f(r)$ and $g(r)$ stand for the blacking functions which depend on the variable r . Following [1, 52], the Hamiltonian describing a massless photon moving reads as

$$\mathcal{H} = \frac{1}{2} g^{ij} p_i p_j = 0. \quad (2)$$

Considering a photon motion on the equatorial plane required by $\theta = \pi/2$, Eq.(2) reduces to

$$\frac{1}{2} \left[-\frac{p_t^2}{f(r)} + g(r)p_r^2 + \frac{p_\phi^2}{r^2} \right] = 0. \quad (3)$$

Since Hamiltonian does not depend explicitly on the coordinates t and ϕ , the associated two constants of motion can be written as

$$p_t \equiv \frac{\partial \mathcal{H}}{\partial \dot{t}} = -\mathcal{E} \quad \text{and} \quad p_\phi \equiv \frac{\partial \mathcal{H}}{\partial \dot{\phi}} = \mathcal{J}. \quad (4)$$

In this way, the quantities \mathcal{E} and \mathcal{J} are considered as the energy and the angular momentum of the photon, respectively. Exploiting the Hamiltonian formalism, the associated equations of motion are

$$\dot{t} = \frac{\partial H}{\partial p_t} = -\frac{p_t}{f(r)}, \quad \dot{\phi} = \frac{\partial H}{\partial p_\phi} = \frac{p_\phi}{r^2}, \quad \text{and} \quad \dot{r} = \frac{\partial H}{\partial p_r} = p_r g(r), \quad (5)$$

Here, the over dot is the derivative with respect to the affine parameter τ and p_r is the radial momentum. They provide a complete description of the dynamics where the effective potential reads as

$$V_e(r) + \dot{r}^2 = 0, \quad (6)$$

from which one obtains

$$V_e(r) = g(r) \left[\frac{\mathcal{J}^2}{r^2} - \frac{\mathcal{E}^2}{f(r)} \right]. \quad (7)$$

It is worth nothing that the photon spherical geometry is associated with the constraints

$$V_e(r_p) = 0, \quad \left. \frac{\partial V_e(r)}{\partial r} \right|_{r=r_p} = 0 \quad \text{and} \quad \left. \frac{\partial^2 V_e(r)}{\partial r^2} \right|_{r=r_p} > 0. \quad (8)$$

It has been shown that this produces an equation parameterizing the orbit of the photon

$$\frac{dr}{d\phi} = \frac{\dot{r}}{\dot{\phi}} = \frac{r^2 g(r) p_r}{\mathcal{J}}. \quad (9)$$

Using Eq.(3), an explicit form for the Eq.(9) can be obtained as follows

$$\frac{dr}{d\phi} = \pm r \sqrt{g(r) \left[\frac{r^2 \mathcal{E}^2}{f(r) \mathcal{J}^2} - 1 \right]}. \quad (10)$$

The turning point of the photon orbit being interpreted mathematically by the constraint $\left. \frac{dr}{d\phi} \right|_{r=R} = 0$ gives

$$\frac{dr}{d\phi} = \pm r \sqrt{g(r) \left[\frac{r^2 f(R)}{f(r) R^2} - 1 \right]}. \quad (11)$$

For later use, we consider a light ray sending from a static observer placed at r_o and transmitting into the past with an angle α with respect to the radial direction. In this way, we have

$$\cot \alpha = \frac{\sqrt{g_{rr}}}{\sqrt{g_{\phi\phi}}} \left. \frac{dr}{d\phi} \right|_{r=r_o} = \frac{1}{r \sqrt{g(r)}} \left. \frac{dr}{d\phi} \right|_{r=r_o}. \quad (12)$$

Exploiting Eq.(11), one obtains

$$\cot^2 \alpha = \frac{r_o^2 f(R)}{f(r_o) R^2} - 1, \quad \sin^2 \alpha = \frac{f(r_o) R^2}{r_o^2 f(R)}. \quad (13)$$

In this context, one gets the angular radius of the black hole shadow by sending R to r_p being the circular orbit radius of the photon appearing in Eq.(8). Precisely, the shadow radius of the black hole observed by a static observer placed at r_o is given by

$$r_s = r_o \sin \alpha = R \sqrt{\frac{f(r_o)}{f(R)}} \Big|_{R=r_p}. \quad (14)$$

According to [1], a link between the black hole shadows and the black hole thermodynamics has been established. Exploiting the heat capacity

$$C = T \left(\frac{\partial S}{\partial T} \right) \quad (15)$$

and using the fact that the entropy is related to event horizon by $S = \pi r_h^2$, with $\frac{\partial S}{\partial r_h} > 0$, the sign of C is directly deduced from the one of $\frac{\partial T}{\partial r_h}$. The computation leads to

$$\frac{dT}{dr_h} = \frac{dT}{dr_s} \frac{dr_s}{dr_h}. \quad (16)$$

When the constraint $\frac{dr_s}{dr_h} > 0$ is satisfied, one can consider

$$\text{Sgn}(C) = \text{Sgn} \left(\frac{\partial T}{\partial r_s} \right). \quad (17)$$

Having discussed the associated shadow backgrounds, we move to prob the link between the shadow radius of the black hole and its phase transition structure including the Van der Waals like phase one. To do so, we consider an AdS black hole solution with a charge Q corresponding to the following blackening function

$$f(r) = g(r) = 1 - \frac{2M}{r} + \frac{Q^2}{r^2} + \frac{8\pi P r^2}{3}, \quad (18)$$

where M is the corresponding mass. It is noted that P is linked to the AdS radius ℓ via $P = \frac{3}{8\pi\ell^2}$ [44, 46]. The event horizon is associated with the large root of the equation $f(r)|_{r=r_h} = 0$, while the Hawking temperature is obtained from the relation

$$T = \frac{f'(r)}{4\pi} \Big|_{r=r_h} = \frac{1}{4\pi r_h} - \frac{Q^2}{4\pi r_h^3} + 2Pr_h. \quad (19)$$

The heat capacity can be expressed as

$$C = \frac{2\pi r_h^2 (8\pi P r_h^4 - Q^2 + r_h^2)}{8\pi P r_h^4 + 3Q^2 - r_h^2}. \quad (20)$$

Using the constraint on the effective potential Eq.(8), we can obtain the formula of the photon circular orbit radius

$$r_p = \frac{1}{2} \left(3M + \sqrt{9M^2 - 8Q^2} \right). \quad (21)$$

It follows that this does not depend on the AdS radius ℓ . Eq.(14) allows one to get the RN-AdS black hole shadow as follows

$$r_s = \frac{\sqrt{6f(r_o)}Q \left(\sqrt{9M^2 - 8Q^2} + 3M \right)}{\sqrt{9M^2 (32\pi PQ^2 - 1) + 3M\sqrt{9M^2 - 8Q^2} (32\pi PQ^2 + 1) + 4Q^2 (3 - 32\pi PQ^2)}}. \quad (22)$$

An observer at spatial infinity can be mathematically translated by imposing the constraint $f(r_0) = 1$, giving the following form of the shadow radius

$$r_s = \frac{\sqrt{6}Q \left(\sqrt{9M^2 - 8Q^2} + 3M \right)}{\sqrt{9M^2 (32\pi PQ^2 - 1) + 3M\sqrt{9M^2 - 8Q^2} (32\pi PQ^2 + 1) + 4Q^2 (3 - 32\pi PQ^2)}} \quad (23)$$

In the vanishing limit of pressure/cosmological constant $P \rightarrow 0$, associated with a large AdS spacetime radius $\ell \rightarrow \infty$, we recover the result reported in [1]. To check the condition $\frac{dr_s}{dr_h} > 0$ from Eq.(16), we illustrate the variation of the shadow radius r_s in terms of the horizon radius r_h in Fig.1. It follows from this figure that r_s increases in terms of r_h ensuring that the positivity of the first derivative of r_s with respect of r_h . Eq.(16) shows that the temperature exhibits similar behaviors for both variables r_s and r_h .

The rest of paper is the main investigation part. In particular, we study the phase transition of AdS black holes using shadow analysis.

3 Phase transition of charged AdS black hole using shadow formalism

In this section, we would like to investigate the phase transition of four-dimensional charged AdS black hole using shadow formalism. Considering the temperature expression Eq.(19) and the heat capacity Eq.(20), we can plot the isobar curves on the $T - r_{h,s}$ and $C - r_{h,s}$, respectively¹ for a fixed value of the charge Q . The plots are depicted in Fig.2. They

¹The subscript indices $_h$ and $_s$ are associated with the event horizon radius and the black hole shadow radius, respectively.

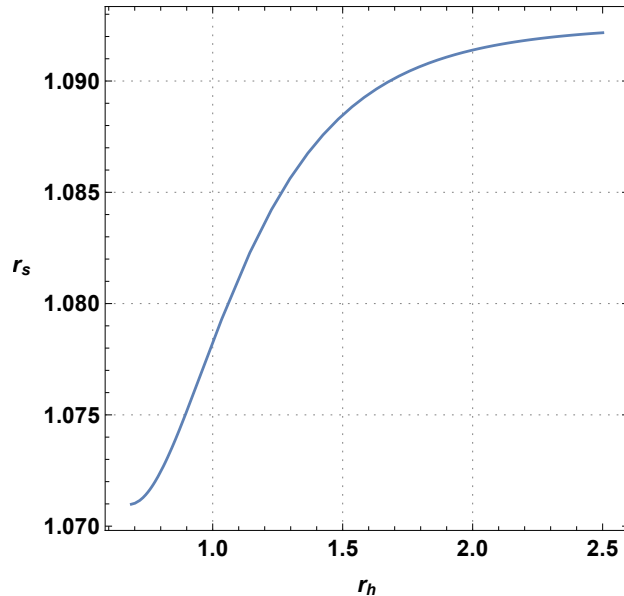


Figure 1: The variation of shadow radius r_s in terms of the event horizon radius r_h , here we have set $Q = 1$ and $P = 0.1$.

show obviously similarities with the Van der Waals phase transitions. It follows that, for different pressure, such curves behave differently. For the large values of pressure $P > P_c$, the temperature involves monotonic behaviors. While, the heat capacity is a continuous function for both variables r_h and r_s . For small pressures $P < P_c$, however, we can observe that the temperature curves are not monotonic. An examination, either on Eq.(20) or on Fig.2, shows that the specific heat capacity changes its sign. Concretely, it changes from positive to negative and then it becomes positive again. For an intermediate range of event horizon/shadow radius (r_h/r_s), the black hole is thermodynamically unstable. In fact, there are three black holes competing thermodynamically. The smallest black hole associated with the domain $[0, r_{h_1, s_1}]$ continues to win until the coexistence temperature T_* . Above such a temperature, the system is considered as a large black hole associated with the interval $[r_{h_1, s_2}, \infty]$. To remove the unstable intermediate branch associated with the domain $[r_{h_1, s_1}, r_{h_2, s_2}]$, we can easily verify the so-called construction of the Maxwell's equal-area interpreted in each plan by

$$\begin{cases} T_*(r_{h_2} - r_{h_1}) = \int_{r_{h_2}}^{r_{h_1}} T dr_h, \\ T_*(r_{s_2} - r_{s_1}) = \int_{r_{s_2}}^{r_{s_1}} T dr_s \end{cases} \quad (24)$$

These two equalities are illustrated in Fig.2 by the two colored surfaces \mathcal{A}_1 and \mathcal{A}_2 in each top panel. The Eqs.(24) are equivalent geometrically to $\mathcal{A}_1 = \mathcal{A}_2$, showing that the system exhibits a phase transition being a first-order one. In the case of $P = P_c$, the smallest black hole and the largest one merge into one squeezing out the unstable black hole. It has been observed an inflection point in the $T - r_{h,s}$ planes, being indicated by dashed lines of Fig.2. At such a point, the specific heat capacity is divergent revealing that this phase transition undergoes a second-order phase transition. In this way, the critical thermodynamical quantities can be obtained by the help of the following equations

$$\left. \frac{\partial T}{\partial r_{h,s}} \right|_{P,Q} = \left. \frac{\partial^2 T}{\partial r_{h,s}^2} \right|_{P,Q} = 0. \quad (25)$$

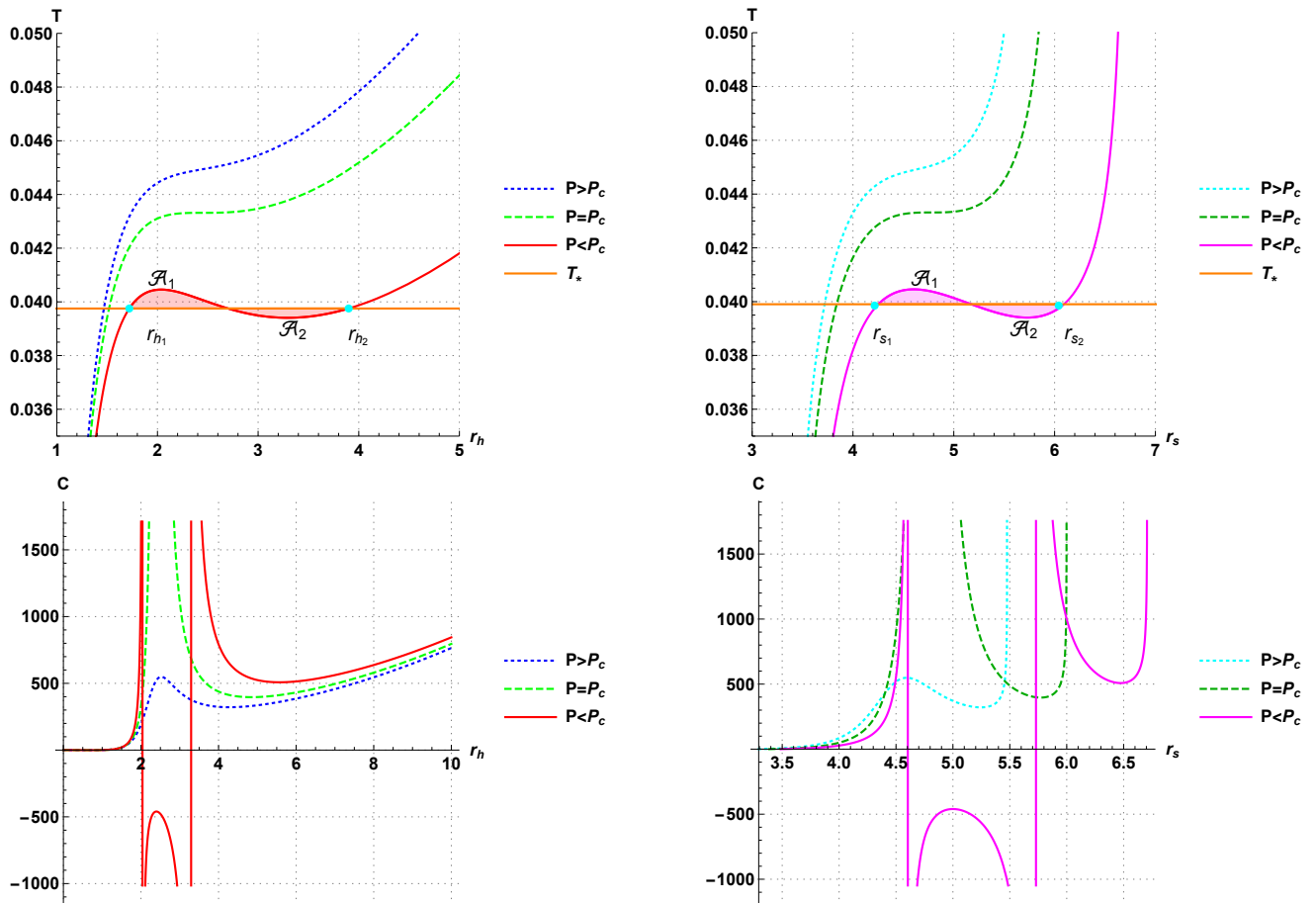


Figure 2: **Top:** The relation between horizon radius r_h (left), shadow radius r_s (right) and temperature for different values of the pressure. The solid line corresponds to the location of the first-order phase transition, while the dashed line to the second-order one. T_* is the coexistence temperature. **Bottom:** The heat capacity versus r_h (left) and r_s (right) for different values of the pressure. For all panels, we have set the charge $Q = 1$.

Substituting Eq.(19) into Eq.(25), we can find certain critical quantities. Indeed, the critical pressure, the critical event horizon radius and the critical temperature are given by

$$P_c = \frac{1}{96\pi Q}, \quad r_{h_c} = \sqrt{6}Q \quad \text{and} \quad T_c = \frac{1}{3\sqrt{6}\pi Q}. \quad (26)$$

These give a critical shadow radius which reads as

$$r_{s_c} = 3\sqrt{\frac{1}{23} \left(29 + 12\sqrt{6} \right)} Q \approx 4.78014Q. \quad (27)$$

It has been remarked that the thermodynamical behaviors in $T - r_h$ and $T - r_s$ planes share many similarities. This could open new gates to prob the phase picture of RN-AdS black holes in terms of their shadows.

To go beyond such an investigation, we examine the behavior of the shadow radius near the second-order phase transition. To see how this works, we evaluate the critical exponent

associated with such a radius. Indeed, we first introduce the following reduced quantities associated with the temperature, the event horizon radius r_h and the shadow radius r_s

$$\tilde{T} = \frac{T}{T_c}, \quad \tilde{r}_h = \frac{r_h}{r_{hc}} \quad \text{and} \quad \tilde{r}_s = \frac{r_s}{r_{sc}} \quad (28)$$

which are obtained from Eq.(19), Eq.(26) and Eq.(23). Then, we determine the width of the coexistence lines. Concretely, we analyze the behavior of the shadow radius $\Delta\tilde{r}_s$

$$\Delta\tilde{r}_s = \tilde{r}_{s_2} - \tilde{r}_{s_1} \quad (29)$$

before and after the second-order small-large black hole phase transition in $\tilde{T} - \tilde{r}_s$ diagram. In the left panel of Fig.3, we illustrate the difference $\Delta\tilde{r}_s$ as a function of the reduced temperature \tilde{T} . It turns out that this allows one to interpret $\Delta\tilde{r}_s$ as an order parameter corresponding to the phase transition of the small-large black holes. As expected, the width of the coexistence line decreases with the reduced temperature, having non zero values at the first-order phase transition. However, it shrinks at the critical point. A close inspection around the second-order phase transition in the right panel of Fig.3 shows that the concavity of the graph is reversed. In particular, it is almost convex at the first-order phase transition. However, near the critical one T_c , it becomes concave.

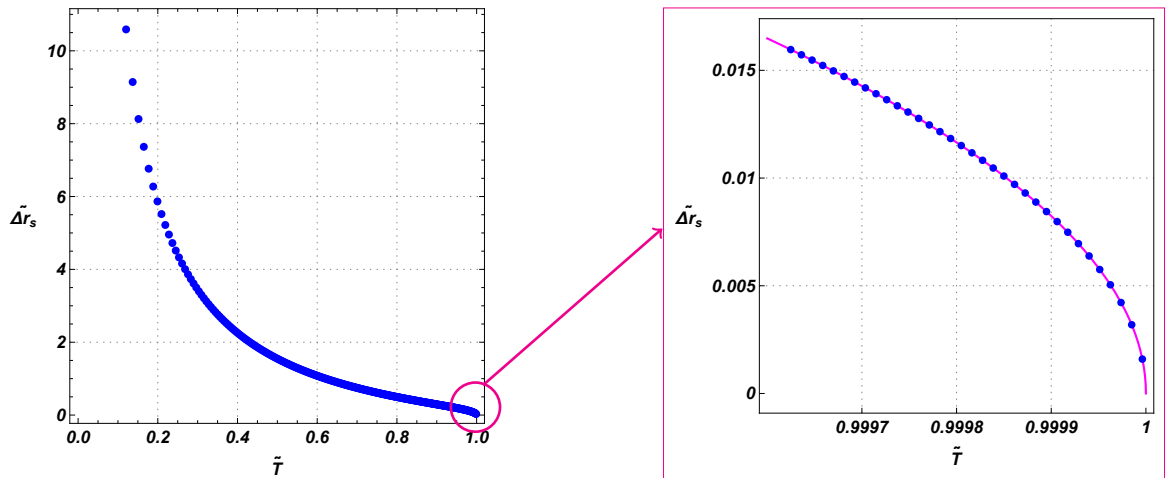


Figure 3: **Left:** The $\Delta\tilde{r}_s$ as function of reduced temperature \tilde{T} . **Right:** Fitting curves $\Delta\tilde{r}_s$ versus \tilde{T}_* near the critical temperature. For both panels we have set $Q = 1$.

To check the consistency of such a finding, we compute the critical exponent characterizing the universal behavior of the reduced differences $\Delta\tilde{r}_s$ around the second-order phase transition. Precisely, we numerically fit the data according to the form

$$\Delta\tilde{r}_s \sim \xi (1 - \tilde{T})^\zeta. \quad (30)$$

Indeed, we can provide a relation between the reduced black hole shadow radius and the reduced temperature near T_c . It is given by

$$\Delta\tilde{r}_s \simeq 0.824796(1 - \tilde{T})^{0.500102}. \quad (31)$$

Under such a numerical accuracy, we can obviously claim that the shadow radius around RN-AdS black hole reveals an universal critical exponent being close to 1/2. Moreover, we can check the concavity of the graphs shown in the left panel of Fig.3 near the critical temperature. Using the derivation of Eq. (30)

$$\frac{d^2 \Delta \tilde{r}_s}{d\tilde{T}^2} = -\xi \zeta (1 - \zeta) (1 - \tilde{T})^{\zeta-2} < 0, \quad (32)$$

the graph must be strictly concave when T goes to T_c . We expect that the detection of concavity change can be considered as signatures of an uncovered criticality. Therefore, the black hole shadow radius could be used to unveil the Van der Waals-like phase transition in RN-AdS black hole backgrounds.

4 Thermal profile on the shadow silhouette of RN-AdS black hole

In this section, we would like to build the so-called thermal image of such a shadow black hole in order to show that the complete Van der Waals-like phase picture reported in [44] via revisited $T - r_h$ curve and within $T - r_s$ diagrams of Fig.2 can be reflected in the thermal profile.

To visualise the shadow boundary curve, we can exploit the stereographic projection in terms of the cartesian coordinates (x, y) , reported in [21], using the following equations

$$x = \lim_{r \rightarrow \infty} \left(-r^2 \sin \theta_0 \frac{d\phi}{dr} \right)_{\theta_0 \rightarrow \frac{\pi}{2}} \quad (33)$$

$$y = \lim_{r \rightarrow \infty} \left(r^2 \frac{d\theta}{dr} \right)_{\theta_0 \rightarrow \frac{\pi}{2}}. \quad (34)$$

Indeed, we provide the behaviour of the shadow circular shape of the RN-AdS black hole for different values of the pressure seen by an observer situated at r_o and an angle α . This is illustrated in Fig.4 for a fixed value of the charge Q . It has been observed that the size of the circular shape of the black hole shadow depends on the pressure. Concretely, it becomes large when $P < P_c$. However, it decreases as P increase. To unveil more information on such an analysis of the black hole phase structure and its shadow, we implement the temperature in order to produce a thermal image. To do so, we consider separately the shadow silhouette for the $P < P_c$, $P = P_c$ and $P > P_c$ cases. By the use of existing map between the polar and the cartesian coordinates, we turn on the temperature variation in terms of r_s on the shadow circular shape. This effect is plotted in Fig.5.

It is noted that the Fig.5 is built from the superposition of each graph from the top-right panel of Fig.2 and its associated circular shape presented in Fig.4. A close examination shows that one has the following findings corresponding to the above three situations $P < P_c$, $P = P_c$ and $P > P_c$.

- Case $P > P_c$ (Top right panel):

It has been seen that the temperature increase monotonically from the center of the shadow (cold region) to its boundary (hot region), which matches perfectly with Cyan curve of Fig.2.

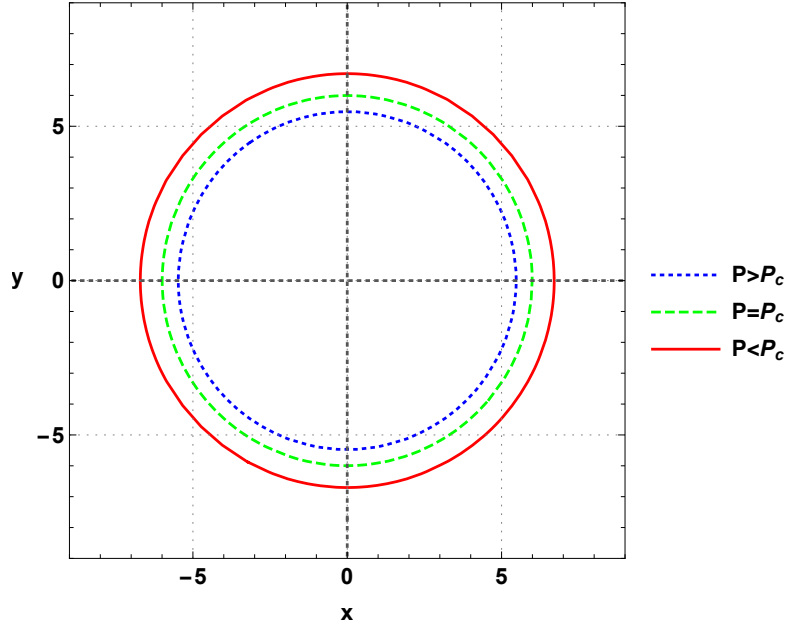


Figure 4: Apparent shape of the charged AdS black hole, as seen by an observer at $(r_o, \alpha = \frac{\pi}{2})$ for different values of the thermodynamical pressure P . Here we have set the mass $M = 60$ and the charge $Q = 1$.

- Case $P = P_c$ (Top middle panel):

The variation is also an increasing in terms of r_s . In this case, the stagnation near the critical point is interpreted by the large light bluish zone being consistent with the dashed green curve appearing in Fig.2. The dotted-dashed line corresponds to the critical temperature.

- $P < P_c$. (Top left panel)

The global variation of the temperature in small and large domains is clearly disclosed within the color gradient of the bar-legend. However, the most relevant discussed case is associated with the temperature. This reveals an oscillator behavior between the points r_{s_1} and r_{s_2} of the red curve in Fig.2 being originated from the Maxwell construction. This behavior can be also observed from the thermal image where the radius $r_{s_{1,2}}$ are represented by the dashed and the dotted circles respectively. At first sight, it is not evident to distinguish the oscillation behavior. To overcome that, a deeper zoom is realized in the down panels of Fig.5. Decoding the bar-legend, it has been remarked that the variation of the color passes from blue ($T = T_* = 0.0397$) to red ($T = 0.0410$) and to darker violet ($T = 0.0390$). Then, it becomes again blue. This shows that the intermediate phase, where the small and large black holes coexist, is distinctly persisting in the thermal profile.

We believe that the obtained results could be seen as a powerful observational tool to probe the thermodynamics of such a black hole associated with experiment activities including LIGO, VIRGO and especially the Event horizon telescope. It is known that the astrophysical black holes are modeled by the Kerr or Schwarzschild black hole configurations. In the light of $M87^*$ observational parameters, we try to depict a naive version of the thermal profile associated with such a black hole. First, we assume that the $M87^*$ corresponds to a Schwarzschild black hole type by setting $Q = P = 0$ in the metric equation Eq.(18). Under such considerations, the event horizon, the Hawking temperature and the shadow radius

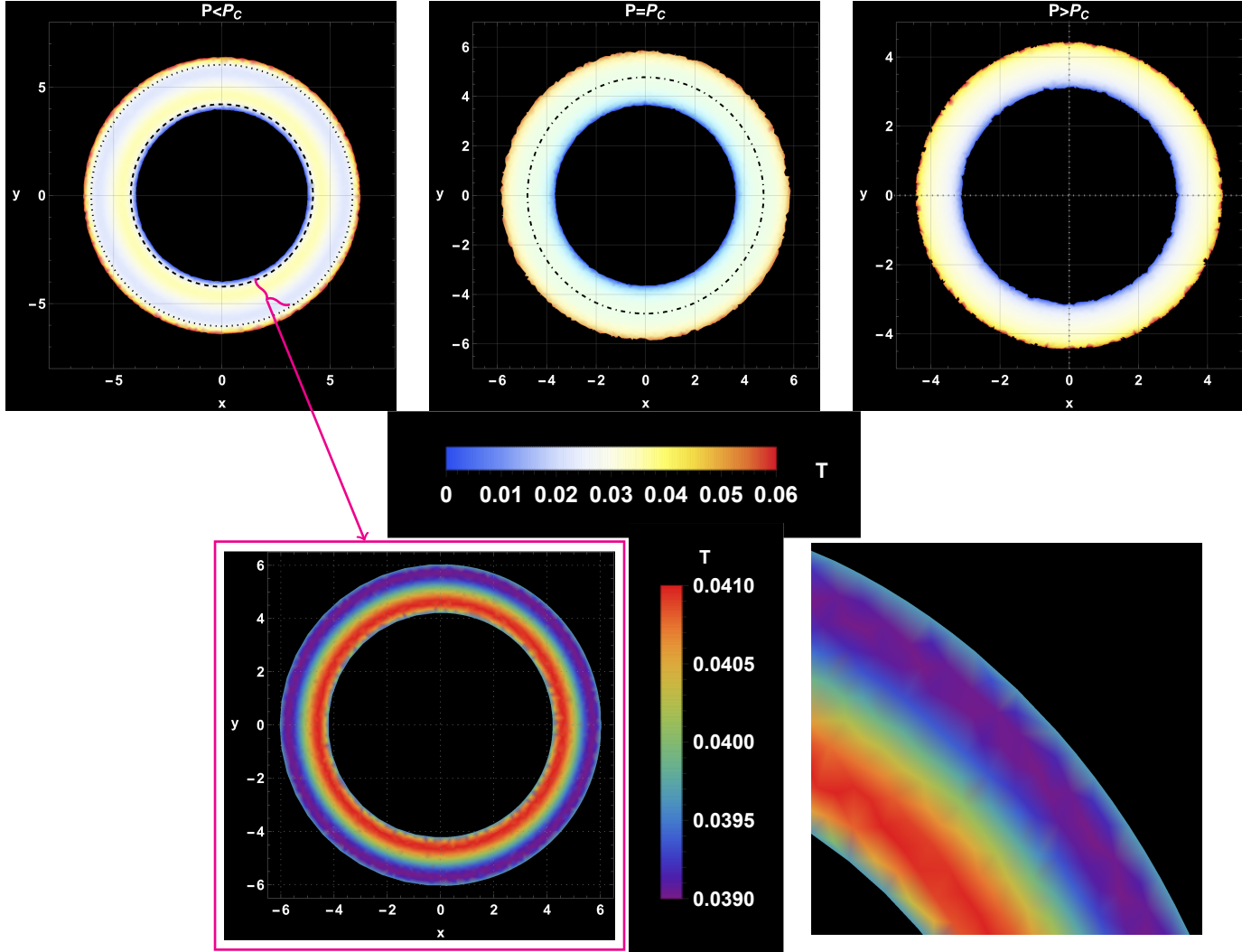


Figure 5: *Superposition of the temperature profile on the silhouette of the shadow cast by the RN-AdS black hole for each thermodynamical case. We have set $M = 60$, and $Q = 1$.*

become respectively

$$r_h = 2M, \quad T = \frac{1}{4\pi r_h} \quad \text{and} \quad r_s = 3\sqrt{3}M. \quad (35)$$

The Event Horizon Telescope data reveals that the $M87^*$ black hole involves a mass $M = (6.5 \pm 0.7) \times 10^9 M_\odot$ and a ring of a diameter $\theta_d = 42 \pm 3 \mu\text{as}$ [3, 4]. With future improvements of the observations, one can have more key pieces of information about the nature of the black hole space-time. The same analysis of the previous sections giving the thermal profile is illustrated in Fig.6

The left panel ensures the validity of this method in the case of Schwarzschild background by checking the condition $\frac{dr_s}{dr_h} > 0$. In the middle panel, we have depicted the variation of such a black hole within the event horizon radius r_h and shadow one r_s . we can easily see that the temperature shares the same decreasing behaviour in terms of $r_{h,s}$. Lastly, we superpose the variation of temperature on the shadow circular shape to built the thermal

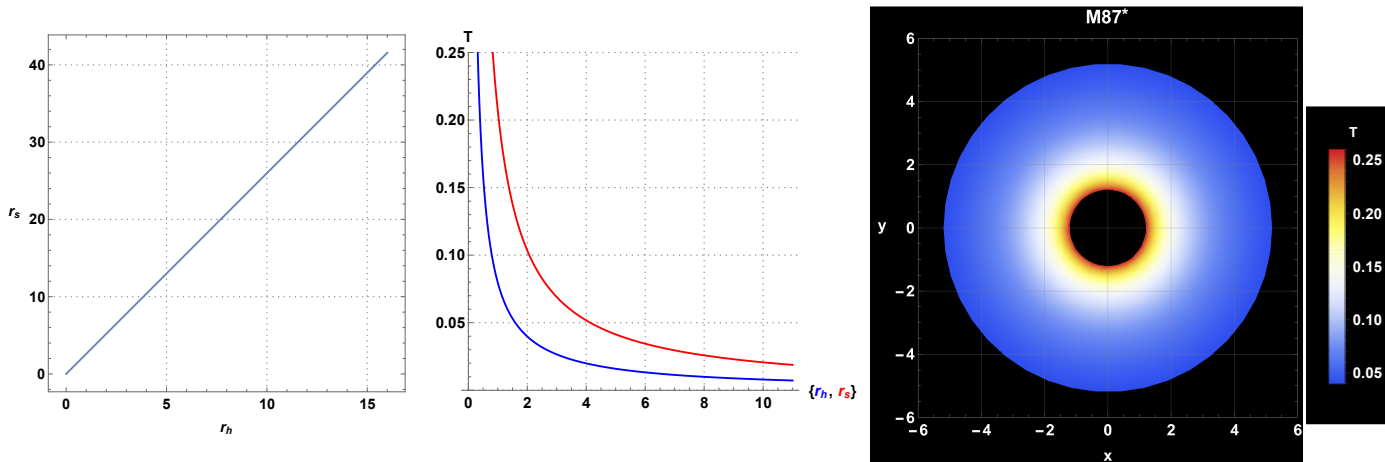


Figure 6: *Building a thermal profile for M87* shadow, by Schwarzschild model and using $M = 1$ in units of the M87* black hole mass given by $M_{BH} = 6.5 \times 10^9 M_{\odot}$ and $r_0 = 91.2 kpc$ [61].*

profile of the M87* under such assumptions. In this regard, we can notice that the centre of black hole shadow is hot than its boundary where the temperature approaches zero.

5 Conclusion

In this work, we have investigated the shadow of charged AdS black holes being considered as a new way to probe the Van der Waals-like phase picture in the extended phase space. Using Hamiltonian formalism, we have, first, exploited the equations of motion controlling the photon dynamics associated with the equatorial plane in such curved backgrounds to build the associated shadow circular shape. Then, nice similarities in the context of phase transition portrait between (T, r_h) and (T, r_s) have been established. For pressure values under the critical one ($P = P_c$), the oscillatory curve of the temperature in terms of r_s as of r_h has provided the presence of a coexistence region for small/large black holes showing that the system undergoes a first-order phase transition. For the second-order phase transition, however, the numerical calculations of the critical exponent in $\Delta \tilde{r}_s - \tilde{T}$ diagram have generated a value being close to $1/2$ which matches perfectly with the Van der Waals fluid systems. To support the present study, we have built a thermal image of such a black hole by varying the temperature on the shadow circular shape. In such an image, we have observed clearly the critical behaviors of RN-AdS black hole solutions in the extended phase space.

This work comes up with certain open questions. Among others, it will be interesting to consider rotating and dS black hole solutions. Motivated by EHT image and its related observational data, it could be possible to build a thermal image of real astronomical black holes. Such questions might be addressed in future works.

Acknowledgements

This work is partially supported by the ICTP through AF-13.

References

- [1] M. Zhang and M. Guo [arXiv:1909.07033 \[gr-qc\]](#).
- [2] Event Horizon Telescope Collaboration (K. Akiyama et al.), *Astrophys. J.* **875**, L1 (2019), [arXiv:1906.11238 \[astro-ph.GA\]](#), doi:10.3847/2041-8213/ab0ec7.
- [3] Event Horizon Telescope Collaboration (K. Akiyama et al.), *Astrophys. J. Lett.* **875**, L6 (2019), [arXiv:1906.11243 \[astro-ph.GA\]](#), doi:10.3847/2041-8213/ab1141.
- [4] Event Horizon Telescope Collaboration (K. Akiyama et al.), *Astrophys. J. Lett.* **875**, L5 (2019), [arXiv:1906.11242 \[astro-ph.GA\]](#), doi:10.3847/2041-8213/ab0f43.
- [5] LIGO Scientific, Virgo Collaboration (B. Abbott et al.), *Phys. Rev. Lett.* **116**, 061102 (2016), [arXiv:1602.03837 \[gr-qc\]](#), doi:10.1103/PhysRevLett.116.061102.
- [6] P. V. P. Cunha, C. A. R. Herdeiro and E. Radu, *Universe* **5**, 220 (2019), [arXiv:1909.08039 \[gr-qc\]](#), doi:10.3390/universe5120220.
- [7] S. Vagnozzi and L. Visinelli, *Phys. Rev. D* **100**, 024020 (2019), [arXiv:1905.12421 \[gr-qc\]](#), doi:10.1103/PhysRevD.100.024020.
- [8] A. Allahyari, M. Khodadi, S. Vagnozzi and D. F. Mota, *JCAP* **02**, 003 (2020), [arXiv:1912.08231 \[gr-qc\]](#), doi:10.1088/1475-7516/2020/02/003.
- [9] J. Synge, *Monthly Notices of the Royal Astronomical Society* **131**, 463 (1966).
- [10] J.-P. Luminet, *Astronomy and Astrophysics* **75**, 228 (1979).
- [11] S. Hawking, B. Carter, J. M. Bardeen, H. Gursky, K. S. Thorne, R. Ruffini, I. D. Novikov et al., *Black holes* (CRC Press, 1973).
- [12] A. De Vries, *Classical and Quantum Gravity* **17**, 123 (2000).
- [13] K. Hioki and U. Miyamoto, *Phys. Rev. D* **78**, 044007 (2008), [arXiv:0805.3146 \[gr-qc\]](#), doi:10.1103/PhysRevD.78.044007.
- [14] P.-C. Li, M. Guo and B. Chen, *Phys. Rev. D* **101**, 084041 (2020), [arXiv:2001.04231 \[gr-qc\]](#), doi:10.1103/PhysRevD.101.084041.
- [15] M. Guo, S. Song and H. Yan, *Phys. Rev. D* **101**, 024055 (2020), [arXiv:1911.04796 \[gr-qc\]](#), doi:10.1103/PhysRevD.101.024055.
- [16] R. Shaikh, P. Kocherlakota, R. Narayan and P. S. Joshi, *Mon. Not. Roy. Astron. Soc.* **482**, 52 (2019), [arXiv:1802.08060 \[astro-ph.HE\]](#), doi:10.1093/mnras/sty2624.
- [17] A. Grenzebach, V. Perlick and C. Lämmerzahl, *Phys. Rev. D* **89**, 124004 (2014), [arXiv:1403.5234 \[gr-qc\]](#), doi:10.1103/PhysRevD.89.124004.
- [18] S. Haroon, M. Jamil, K. Jusufi, K. Lin and R. B. Mann, *Phys. Rev. D* **99**, 044015 (2019), [arXiv:1810.04103 \[gr-qc\]](#), doi:10.1103/PhysRevD.99.044015.

- [19] T. Johannsen, A. E. Broderick, P. M. Plewa, S. Chatzopoulos, S. S. Doeleman, F. Eisenhauer, V. L. Fish, R. Genzel, O. Gerhard and M. D. Johnson, *Phys. Rev. Lett.* **116**, 031101 (2016), [arXiv:1512.02640 \[astro-ph.GA\]](#), doi:10.1103/PhysRevLett.116.031101.
- [20] P. V. P. Cunha, C. A. R. Herdeiro, E. Radu and H. F. Runarsson, *Phys. Rev. Lett.* **115**, 211102 (2015), [arXiv:1509.00021 \[gr-qc\]](#), doi:10.1103/PhysRevLett.115.211102.
- [21] E. F. Eiroa and C. M. Sendra, *Eur. Phys. J.* **C78**, 91 (2018), [arXiv:1711.08380 \[gr-qc\]](#), doi:10.1140/epjc/s10052-018-5586-6.
- [22] M. Wang, S. Chen and J. Jing, *Phys. Rev.* **D97**, 064029 (2018), [arXiv:1710.07172 \[gr-qc\]](#), doi:10.1103/PhysRevD.97.064029.
- [23] N. Tsukamoto, *Phys. Rev.* **D97**, 064021 (2018), [arXiv:1708.07427 \[gr-qc\]](#), doi:10.1103/PhysRevD.97.064021.
- [24] O. Yu. Tsupko, *Phys. Rev.* **D95**, 104058 (2017), [arXiv:1702.04005 \[gr-qc\]](#), doi:10.1103/PhysRevD.95.104058.
- [25] M. Sharif and S. Iftikhar, *Eur. Phys. J.* **C76**, 630 (2016), [arXiv:1611.00611 \[gr-qc\]](#), doi:10.1140/epjc/s10052-016-4472-3.
- [26] T. Ohgami and N. Sakai, *Phys. Rev.* **D94**, 064071 (2016), [arXiv:1704.07093 \[gr-qc\]](#), doi:10.1103/PhysRevD.94.064071.
- [27] Z. Younsi, A. Zhidenko, L. Rezzolla, R. Konoplya and Y. Mizuno, *Phys. Rev.* **D94**, 084025 (2016), [arXiv:1607.05767 \[gr-qc\]](#), doi:10.1103/PhysRevD.94.084025.
- [28] A. Abdujabbarov, M. Amir, B. Ahmedov and S. G. Ghosh, *Phys. Rev.* **D93**, 104004 (2016), [arXiv:1604.03809 \[gr-qc\]](#), doi:10.1103/PhysRevD.93.104004.
- [29] M. Amir and S. G. Ghosh, *Phys. Rev.* **D94**, 024054 (2016), [arXiv:1603.06382 \[gr-qc\]](#), doi:10.1103/PhysRevD.94.024054.
- [30] F. Atamurotov and B. Ahmedov, *Phys. Rev.* **D92**, 084005 (2015), [arXiv:1507.08131 \[gr-qc\]](#), doi:10.1103/PhysRevD.92.084005.
- [31] V. Perlick, O. Yu. Tsupko and G. S. Bisnovatyi-Kogan, *Phys. Rev.* **D92**, 104031 (2015), [arXiv:1507.04217 \[gr-qc\]](#), doi:10.1103/PhysRevD.92.104031.
- [32] J. W. Moffat, *Eur. Phys. J.* **C75**, 130 (2015), [arXiv:1502.01677 \[gr-qc\]](#), doi:10.1140/epjc/s10052-015-3352-6.
- [33] R.-S. Lu, A. E. Broderick, F. Baron, J. D. Monnier, V. L. Fish, S. S. Doeleman and V. Pankratius, *Astrophys. J.* **788**, 120 (2014), [arXiv:1404.7095 \[astro-ph.IM\]](#), doi:10.1088/0004-637X/788/2/120.
- [34] F. Atamurotov, A. Abdujabbarov and B. Ahmedov, *Phys. Rev.* **D88**, 064004 (2013), doi:10.1103/PhysRevD.88.064004.
- [35] M. Guo, N. A. Obers and H. Yan, *Phys. Rev.* **D98**, 084063 (2018), [arXiv:1806.05249 \[gr-qc\]](#), doi:10.1103/PhysRevD.98.084063.

- [36] H. Yan, Phys. Rev. **D99**, 084050 (2019), [arXiv:1903.04382 \[gr-qc\]](#), doi:10.1103/PhysRevD.99.084050.
- [37] R. A. Hennigar, M. B. J. Poshteh and R. B. Mann, Phys. Rev. **D97**, 064041 (2018), [arXiv:1801.03223 \[gr-qc\]](#), doi:10.1103/PhysRevD.97.064041.
- [38] R. A. Konoplya, Phys. Lett. **B795**, 1 (2019), [arXiv:1905.00064 \[gr-qc\]](#), doi:10.1016/j.physletb.2019.05.043.
- [39] C. Bambi and K. Freese, Phys. Rev. **D79**, 043002 (2009), [arXiv:0812.1328 \[astro-ph\]](#), doi:10.1103/PhysRevD.79.043002.
- [40] C. Bambi and N. Yoshida, Class. Quant. Grav. **27**, 205006 (2010), [arXiv:1004.3149 \[gr-qc\]](#), doi:10.1088/0264-9381/27/20/205006.
- [41] R. A. Konoplya, T. Pappas and A. Zhidenko, Phys. Rev. D **101**, 044054 (2020), [arXiv:1907.10112 \[gr-qc\]](#), doi:10.1103/PhysRevD.101.044054.
- [42] C. Bambi, K. Freese, S. Vagnozzi and L. Visinelli, Phys. Rev. D **100**, 044057 (2019), [arXiv:1904.12983 \[gr-qc\]](#), doi:10.1103/PhysRevD.100.044057.
- [43] A. Chamblin, R. Emparan, C. V. Johnson and R. C. Myers, Phys. Rev. **D60**, 064018 (1999), [arXiv:hep-th/9902170 \[hep-th\]](#), doi:10.1103/PhysRevD.60.064018.
- [44] D. Kubiznak and R. B. Mann, JHEP **07**, 033 (2012), [arXiv:1205.0559 \[hep-th\]](#), doi:10.1007/JHEP07(2012)033.
- [45] A. Belhaj, M. Chabab, H. El Moumni and M. B. Sedra, Chin. Phys. Lett. **29**, 100401 (2012), [arXiv:1210.4617 \[hep-th\]](#), doi:10.1088/0256-307X/29/10/100401.
- [46] S. Gunasekaran, R. B. Mann and D. Kubiznak, JHEP **11**, 110 (2012), [arXiv:1208.6251 \[hep-th\]](#), doi:10.1007/JHEP11(2012)110.
- [47] A. Belhaj, M. Chabab, H. El Moumni, K. Masmar, M. B. Sedra and A. Segui, JHEP **05**, 149 (2015), [arXiv:1503.07308 \[hep-th\]](#), doi:10.1007/JHEP05(2015)149.
- [48] S. H. Hendi and M. H. Vahidinia, Phys. Rev. **D88**, 084045 (2013), [arXiv:1212.6128 \[hep-th\]](#), doi:10.1103/PhysRevD.88.084045.
- [49] J.-L. Zhang, R.-G. Cai and H. Yu, Phys. Rev. **D91**, 044028 (2015), [arXiv:1502.01428 \[hep-th\]](#), doi:10.1103/PhysRevD.91.044028.
- [50] S.-W. Wei and Y.-X. Liu, Phys. Rev. Lett. **115**, 111302 (2015), [arXiv:1502.00386 \[gr-qc\]](#), doi:10.1103/PhysRevLett.116.169903,10.1103/PhysRevLett.115.111302, [Erratum: Phys. Rev. Lett.116,no.16,169903(2016)].
- [51] M. Chabab, H. El Moumni and K. Masmar, Eur. Phys. J. **C76**, 304 (2016), [arXiv:1512.07832 \[hep-th\]](#), doi:10.1140/epjc/s10052-016-4155-0.
- [52] V. Perlick, O. Y. Tsupko and G. S. Bisnovatyi-Kogan, Phys. Rev. D **97**, 104062 (2018), [arXiv:1804.04898 \[gr-qc\]](#), doi:10.1103/PhysRevD.97.104062.

- [53] P. H. Nguyen, JHEP **12**, 139 (2015), [arXiv:1508.01955 \[hep-th\]](#), doi:10.1007/JHEP12(2015)139.
- [54] H. El Moumni, Phys. Lett. **B776**, 124 (2018), doi:10.1016/j.physletb.2017.11.037.
- [55] Y. Liu, D.-C. Zou and B. Wang, JHEP **09**, 179 (2014), [arXiv:1405.2644 \[hep-th\]](#), doi:10.1007/JHEP09(2014)179.
- [56] M. Chabab, H. El Moumni, S. Iraoui and K. Masmar, Eur. Phys. J. **C76**, 676 (2016), [arXiv:1606.08524 \[hep-th\]](#), doi:10.1140/epjc/s10052-016-4518-6.
- [57] D.-C. Zou, Y. Liu and R.-H. Yue, Eur. Phys. J. **C77**, 365 (2017), [arXiv:1702.08118 \[gr-qc\]](#), doi:10.1140/epjc/s10052-017-4937-z.
- [58] M. Chabab, H. El Moumni, S. Iraoui, K. Masmar and S. Zhizeh, Phys. Lett. **B781**, 316 (2018), [arXiv:1804.03960 \[hep-th\]](#), doi:10.1016/j.physletb.2018.04.014.
- [59] S.-W. Wei and Y.-X. Liu, Phys. Rev. **D97**, 104027 (2018), [arXiv:1711.01522 \[gr-qc\]](#), doi:10.1103/PhysRevD.97.104027.
- [60] M. Chabab, H. El Moumni, S. Iraoui and K. Masmar, Int. J. Mod. Phys. **A34**, 1950231 (2020), [arXiv:1902.00557 \[hep-th\]](#), doi:10.1142/S0217751X19502312.
- [61] K. Jusufi, M. Jamil, P. Salucci, T. Zhu and S. Haroon, Phys. Rev. D **100**, 044012 (2019), [arXiv:1905.11803 \[physics.gen-ph\]](#), doi:10.1103/PhysRevD.100.044012.